Available online at www.sciencedirect.com
ScienceDirect
Journal of Photochemistry and Photobiology A: Chemistry 193 (2008) 10–17
Journal of Photochemistry and Photobiology A:Chemistry
www.elsevier.com/locate/jphotochem

Interaction of TiO_2 nano-particles with organic UV absorbers

Terry A. Egerton [a], Neil J. Everall [b], John A. Mattinson [a], Lorna M. Kessell [c], Ian R. Tooley [c,*]

[a] *School of Chemical Engineering & Advanced Materials, University of Newcastle upon Tyne, Newcastle upon Tyne NE1 7RU, UK*
[b] *ICI Measurement Science Group, Wilton Research Centre, Wilton, Redcar TS10 4RF, UK*
[c] *Croda R&D, Wilton Research Centre, Wilton, Redcar TS10 4RF, UK*

Received 14 March 2007; received in revised form 1 June 2007; accepted 1 June 2007
Available online 7 June 2007

Abstract

The yellowing caused by the addition of butyl methoxy dibenzoylmethane (BMDBM), or benzophenone, to dispersions of titania has been measured quantitatively for a range of uncoated and surface-treated nano-particulate TiO_2 materials. FTIR spectra of BMDBM adsorbed on the uncoated titania were interpreted with the aid of corresponding spectra of adsorbed acetyl acetonate and supporting DFT calculations. The IR spectra suggest that chemisorption of BMDBM by bidentate chelation of the diketone anion to surface titaniums is responsible for the observed yellowing.

Silica coatings, deposited on the TiO_2 surface led to a large reduction in yellowing with both BMDBM and benzophenone-3. This was consistent with the coating uniformity and coherence inferred from reduction in the rates of propan-2-ol photo-oxidation. It is proposed that silica coating reduces interactions of butyl methoxy dibenzoylmethane (BMDBM) and benzophenone-3 with the highly polarizing Ti surface cations. A beneficial practical consequence is that aesthetically undesirable discolouration of cosmetic formulations containing combinations of these active ingredients is reduced. Propan-2-ol oxidation suggested that, on the same TiO_2, alumina coatings were less uniform. Patchier coverage led to more yellowing of the titania because it allowed greater access of the organic to the underlying TiO_2. In addition, at low levels of alumina the coating induced *more* yellowing than on the uncoated metal oxide surface. This was attributed to coordination to coordinatively unsaturated aluminiums.

The presence of an organic coating, such as surface bound stearate, further reduced yellowing interactions with organic UV absorbers probably because the stearate competes effectively for (i.e. blocks) surface sites.

Keywords: Titanium dioxide; Organic UV absorbers

1. Introduction

This paper explores the interactions between organic UV absorbers and the surfaces of nano-particulate-coated TiO_2. UV absorbing sunscreen formulations often include both inorganic (e.g. TiO_2) and organic (e.g. butyl methoxy dibenzoylmethane) absorbers which interact to give a yellow colouration. The yellowing is modified by coating the TiO_2 with an inorganic hydrous oxide [1,2] and photocatalysis has been used to probe the coating effectiveness of both silica and alumina.

The surface modification of the nano-particulate titanium dioxide used in sunscreens exemplifies many of the challenges that must be addressed in the surface modification of oxide nano-particles. The surface of the, typically less than 50 nm, TiO_2 is usually modified with a coating of inorganic hydrous oxide to minimise photoactivity [1,2]. An organic surface treatment such as stearate [3] chlorsilane or polysiloxane [4] may be used to optimize particle dispersion in the medium of application and hence minimise scattering of visible (400–700 nm) light and maximise the attenuation of ultraviolet B (290–320 nm) radiation (UVB) [5]. Recently, to provide higher levels of protection from the damaging effects of ultraviolet A (320–400 nm) radiation (UVA) on skin [6], TiO_2 has often been combined with organic UVA absorbers, such as butyl methoxy dibenzoylmethane (BMDBM) and benzophenone-3 [7]. Avoidance of an unacceptable discolouration, yellowing, caused by interaction of such organic absorbers with the TiO_2 introduces a third requirement for the surface coating and provides the background to this study.

The measurement of coating integrity has challenged surface scientists for many years. Analytical methods, such as X-ray fluorescence spectroscopy (XRF), detect the presence of coating

* Corresponding author. Tel.: +44 1642 435467.
E-mail address: ian.tooley@croda.com (I.R. Tooley).

1010-6030/$ – see front matter © 2007 Elsevier B.V. All rights reserved.
doi:10.1016/j.jphotochem.2007.06.001

elements but cannot differentiate between a complete shell around the particle and a separate precipitate of the coating. Electrophoretic measurements can only detect gross changes on a length scale comparable with the Debye Huckel double layer and the coatings are too thin to allow clear results from surface techniques such as electron spectroscopy for chemical analysis XPS (ESCA) [8]. Transmission electron microscopy (TEM) though useful for larger particles is, in our experience, of limited use for ultrafine TiO_2 because the change in electron density is insufficient to differentiate between the particle and the coating. This study builds on earlier studies which demonstrated that, in general, coating inactivated the surface sites responsible for adsorption of IR-active N_2 [1] and both propan-2-ol oxidation [9] and photoreduction of DPPH [10] and photogreying [2]. Those results were used to build up a model of surface coverage and integrity which is now extended to explore the link between the integrity of these coatings and the discolouration of mixtures of the particles with BMDBM and benzophenone-3 in the absence of UV radiation.

2. Experimental

2.1. Materials

2.1.1. Chemicals

The experimental rutile base (BET area $\sim 130 \pm 5\,m^2\,g^{-1}$), sample A of Table 1, was prepared by hydrolysis of $TiCl_4$. Two moles of titanium oxydichloride (equivalent to 5 mol dm^{-3} TiO_2) solution was reacted with 5.5 mol of sodium hydroxide (4.7 mol dm^{-3}) in aqueous solution at 80 °C with stirring. After the 2 h reaction phase was completed the slurry was neutralised by the addition of sodium hydroxide. The slurry was either coated (methods described below) or filtered and washed with deionised water and dried at 110 °C to produced uncoated rutile, sample A. A fine powder was produced from the dried filter cake by a dry powder mill [11].

Table 1
TiO_2 samples and dispersion media used in this study. The numbers in parenthesis refers to the BET N_2 surface area of the materials

Material	Designation	Further details ($m^2\,g^{-1}$)
Uncoated rutile, $\sim 130\,m^2\,g^{-1}$	A	Uniqema, Hydrolysis of $TiCl_4$
Rutile A coated with increasing amounts of silica	B–L	0.1 (111), 0.25 (110), 0.5 (115), 1 (118), 3.2 (121), 5 (110), 6.2, 10 (96), 12.8, 20 (94) and 40 (50) wt.% silica coating, respectively
Rutile A coated with increasing amounts of alumina	M, N, O and P	1 (115), 5 (114), 25 (105) and 40 (75) wt.% alumina coating, respectively
Rutile A coated with 10.5 wt.% silica and increasing amounts of stearate	Q–V	9, 11, 15 and 17 wt.% stearate, respectively
Rutile A coated with 10.5 wt.% alumina and increasing amounts of stearate	W–Z	6.5, 13.5, 20.25 and 27 wt.% stearate, respectively
Mixed alkyl (C_{12}–C_{15}) benzoate	FIN	Goldschmidt (Tegosoft TN)
Propan-2-ol	IPA	Aldrich 99.9% reagent grade

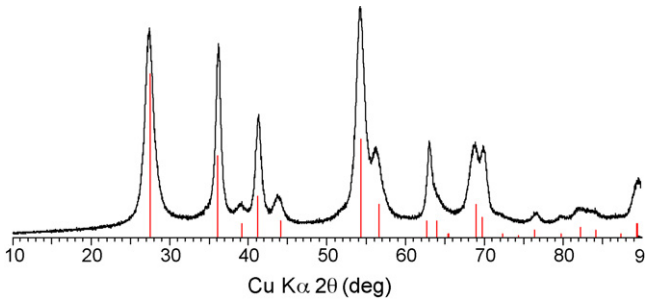

Fig. 1. Diffraction pattern of rutile sample A. The vertical lines show the expected positions of the rutile diffraction maxima.

Diffuse reflectance infrared Fourier transform spectroscopy (DRIFTS) and Attenuated total reflectance Fourier transform infrared spectroscopy (ATR-FTIR) showed the absence of organic contamination on the surface.

Powder X-ray diffraction patterns were measured with Cu Kα radiation in a Siemens D5000 diffractometer equipped with an energy dispersive detector acting as a monochromator. The diffractograms showed no phases other than rutile (Fig. 1). The data was analysed by fitting the diffraction pattern between 22 and 48° 2θ with a set of peaks corresponding to the reflection positions for rutile. A mean crystallite size of ~9 nm was determined for the rutile 1 1 0 reflection (at approximately 27.4° 2θ) based on its integral breadth according to the principles of the method of Stokes and Wilson [12].

Electron microscopy showed that the crystals were lenticular (Fig. 2) and the X-ray size of ~9 nm in the 1 1 0 direction is con-

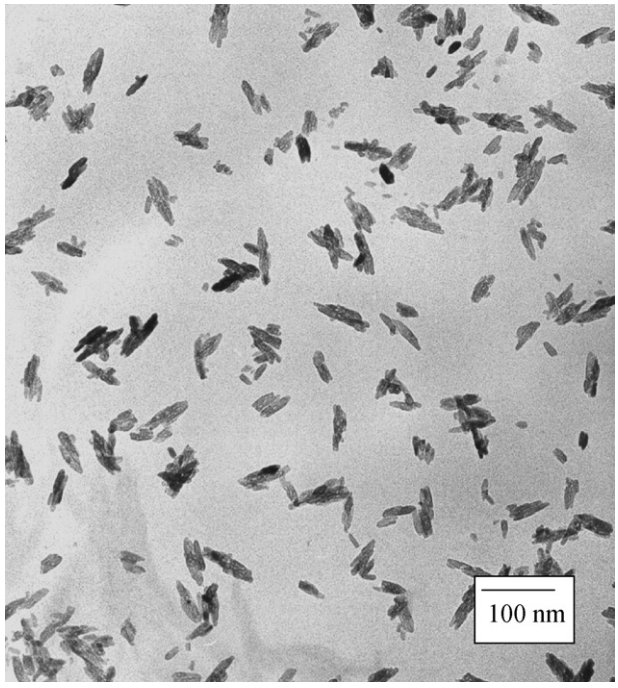

Fig. 2. TEM image of nano-particulate rutile needles.

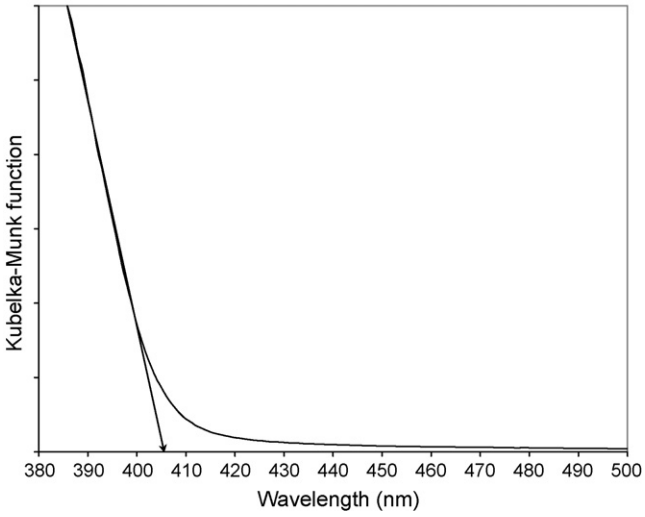

Fig. 3. Diffuse reflectance spectra of untreated rutile plotted as the Kubelka–Munk function. Reflectance measurements were made against a $BaSO_4$ white reference. The arrow indicates the rutile has an absorption edge at 405 nm.

sistent with the particle dimensions revealed by the micrographs [3].

The diffuse reflectance spectrum (Fig. 3) shows that the rutile begins to absorb at ∼405 nm, implying a band gap of 3.0 eV. However transmission spectra of aqueous dispersions show a maximum at ∼280 nm because, as predicted by Mie theory both the absorption and the scattering depend on the ratio of particle size, d, to wavelength λ [13].

All of the surface-modified titanias, B–Z (Table 1), were derived from this rutile base crystal. All solvents/organics were used as received from suppliers.

2.1.2. Silica-modified rutile

Samples B–L were prepared by Iler's dense silica method [14]. A silica coating was applied to a 30 g dm^{-3} suspension of rutile, sample A, in water at pH 9–9.5. One cubic decimeter of TiO_2 slurry was heated to 90 °C and the required quantity of sodium silicate (27 wt.% sodium silicate solution) and 3 mol dm^{-3} hydrochloric acid was added dropwise between pH 9 and 9.5. After the addition, pH was adjusted to 7 by dropwise addition of 3 mol dm^{-3} hydrochloric acid. The product was filtered, washed and dried in air at 110 °C. The surface areas of these silica-coated samples (Table 1) generally decrease with increasing levels of silica.

2.1.3. Alumina-modified rutile

Alumina modification of the TiO_2 surface, samples M–P, was achieved by dropwise addition of caustic sodium aluminate (20 wt.% Al_2O_3) to a slurry (30 g dm^{-3}) of sample A in water at 50 °C [1,3]. The equilibrated alkali slurry was neutralised by controlled addition of hydrochloric acid. The slurry was filtered, washed and dried in the same way as the silica-modified titanias described above. The surface areas of alumina-coated samples also decreased with increasing levels of alumina but the decrease is less than for the silica samples. This is consistent with a more porous coating structure.

2.1.4. Silica + stearate-modified rutile

Sodium silicate solution was added dropwise to 30 g dm^{-3} slurry of TiO_2 suspended in water at 50 °C. The temperature was raised to 75 °C before the required quantity of sodium stearate solution (100 g dm^{-3}) was added. Following equilibration pH was adjusted to 6.5–7.0 by dropwise addition of hydrochloric acid. The effect of stearate on measured surface areas has been discussed in Ref. [3].

2.1.5. Measurement of photocatalytic oxidation of propan-2-ol

Photocatalytic oxidation activity was measured at 30 °C by monitoring the photo-generation of acetone by a dispersion of 0.4 g TiO_2 in 50 ml of neat isopropanol. The reaction was carried out in a cylindrical pyrex vessel illuminated, from the base, by two UV lamps with a maximum output at ∼365 nm (Philips PL-L 36W 09), as previously described [1]. The reaction mixture was sampled by a hypodermic syringe through a port fitted with a septum cap and filtered to remove titanium dioxide. Samples were analysed for acetone by gas chromatography (Cambridge GC94, Chromosorb wax 60/80 mesh at 70 °C) calibrated with mixtures of acetone and propan-2-ol using a diethyl ether internal standard. Straight-line calibration plots (R^2 0.997) were obtained.

2.1.6. Measurement of photogreying

Photogreying was determined by measuring the discolouration of dispersions of titanium dioxide in C_{12}–C_{15} alkyl benzoate The dispersions were prepared by milling the powder at 5 wt.% (silica-coated samples) or 15 wt.% (alumina-coated samples) into the carrier fluid for 15 min at 5000 rpm with a mini-motor mill (Eiger Torrance MK M50 VSE TFV) 70% filled with 0.8–1.25 mm zirconia beads (ER120SWIDE). Freshly milled dispersions were loaded into specially constructed Perspex cells as shown in Fig. 4. A quartz glass cover slip was placed over the sample to eliminate contact with the atmosphere. Up to 12 cells could be placed on a rotating platform, positioned 12 cm from a

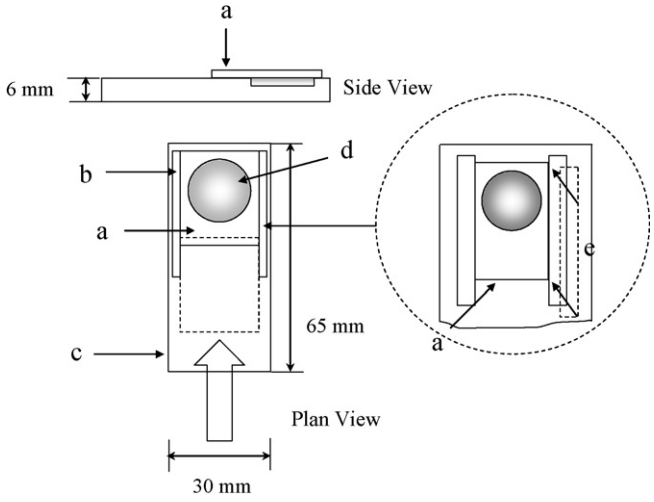

Fig. 4. Schematic diagram of a photogreying cell: (a) quartz glass cover slip, (b) solid brass stopper, (c) pyrex cell, (d) sample holder drilled into pyrex cell, (e) movable brass strip to secure quartz cover slip.

75 W UV light source (Philips HB 171/A with 4 TL29D16/09N lamps) and irradiated for 120 min; sample colour was recorded using the $L^*a^*b^*$ values of the CIE colour system [15]. The reflectance was then reported as the brightness value, L^*, of the Lab colour system at 30 min intervals by a commercial colour meter (Minolta chromameter CR-300), previously calibrated with a standard white tile ($L^* = 97.95$, $b^* = 2$). L^* is related to the relative reflectance $R = (Y/Y_0)$, where Y_0 is the reflectance of a perfect white and b^* is the chromaticity coordinate in the Z direction of the $L^*a^*b^*$ colour system related to yellow ($+b^*$) to blue ($-b^*$) colour differences. Delta L^* ($L^*_{0\text{min}} - L^*_{120\text{min}}$) was taken as a measure of photogreying.

2.1.7. Measurement of yellowing with butyl methoxy bibenzoylmethane (BMDBM) and benzophenone-3

Yellowing of dispersions was determined by thoroughly mixing 1.25 g of organic UV absorber (BMDBM or Benzophenone-3) with 23.75 g of photogreying mixture (15 wt.%, preparation method described above). b^* was measured 30 min after mixing the components together by a colourimeter (Minolta chromameter CR-300). $b^*_{(\text{with organic})} - b^*_{0\ (\text{without organic})}$ was taken as measure of yellowing.

2.1.8. Infrared spectroscopy

TiO_2 complexes were examined by extracting the solid from a mixture of BMDBM and mineral oil (selected because it does not have infrared absorption bands in the region of interest) by blotting the mixture with filter paper to remove excess solvent. The samples were left to dry for several hours at room temperature and compressed in a diamond cell to reduce their thickness. FTIR transmission spectra were recorded by a Nicolet 860 FTIR spectrometer equipped with a Nicplan IR microscope.

3. Results

3.1. Photochemical studies to assess coating coverage

The effect of coating the high area rutile, sample A, with increasing levels of silica or alumina is shown in Fig. 5. At low loadings, alumina had a negligible effect on photoactivity (both propan-2-ol oxidation and photogreying) whereas silica-coated samples showed a slight increase in activity. No attempt has been made to rationalise these small increases which could, for example, be due to changes in particle dispersion with changing surface properties.

At high loadings, both silica and alumina reduced the rate of propan-2-ol oxidation. For a fixed loading of inorganic coating, silica was more effective at reducing photo-oxidation than alumina, as previously reported for a different set of samples [1]. These results confirmed the conclusions of previous experiments [1]; that for an equal weight of coating, silica is more effective than alumina as a physical barrier to photogenerated electrons and holes migrating to the surface of the titanium dioxide nano-particles, which can lead to the formation of $^{\bullet}O_2^-$ and $^{\bullet}OH$ radicals (Eqs. (2) and (3)).

$$TiO_2 + UV \rightarrow e^- + h^+ \quad (1)$$

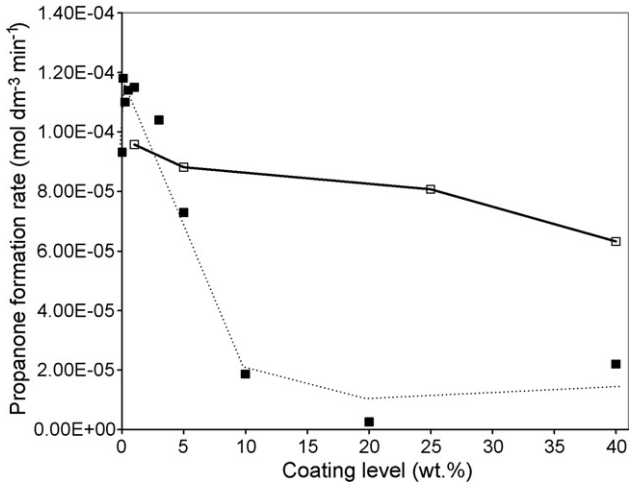

Fig. 5. Rate of propanone formation, by photocatalytic oxidation of propan-2-ol vs. coating level for (■) silica (samples B–L) and (□) alumina (samples M–P) coated titanium dioxide. Sample A was used as the base material in all cases.

$$e^- + O_2 \rightarrow {}^{\bullet}O_2^- \quad (2)$$

$$h^+ + OH^- \rightarrow {}^{\bullet}OH \quad (3)$$

Photogreying (Fig. 6) also decreased with increased coating level and, again, silica was much more effective than an equivalent loading of alumina. The implication is, again, that the coatings increase electron–hole recombination (Eq. (4)) and hence, in the absence of oxygen, reduce reduction of Ti^{4+} to Ti^{3+} (Eq. (5)).

$$e^- + h^+ \rightarrow \text{heat} \quad (4)$$

$$e^- + Ti^{4+} \rightarrow Ti^{3+} \quad (5)$$

The silica was deposited by a method that is known to give a coherent silica coating [8,14]. For the silica-coated samples the rate of propan-2-ol oxidation and the photogreying reached limiting values, of ca. 20% of the uncoated TiO_2, at ~15 wt.% silica.

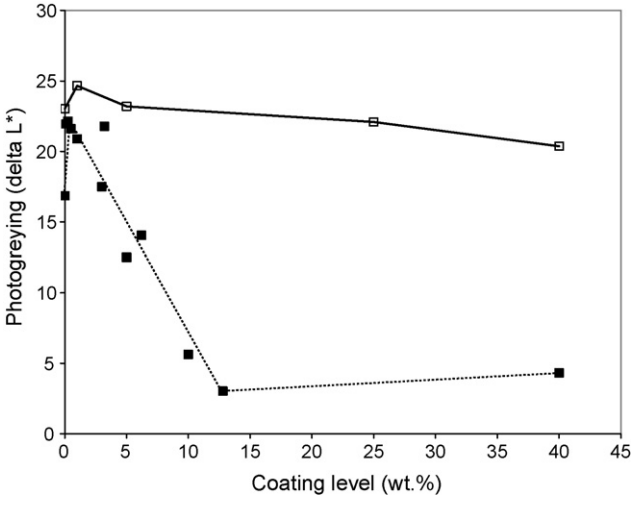

Fig. 6. Photogreying (delta L^*) of dispersions of TiO_2 in C_{12}–C_{15} alkyl benzoate vs. coating level for (■) silica (B–L) and (□) alumina (M–P) coated sample A (silica measured at 5 wt.% loading, alumina measured at 15 wt.% loading).

This implies that at ∼15 wt.% of silica the surface is effectively encapsulated, since the rate of propan-2-ol and the photoreduction in the presence of C_{12}–C_{15} alkyl benzoate approach a limiting value. The surface area of ∼130 $m^2\ g^{-1}$ corresponds to an equivalent sphere diameter of 10 nm and simple calculations based on a coherent skin of density 2.13 $g\ cm^{-3}$ applied to identical 10 nm diameter spheres of density 4.26 $g\ cm^{-3}$ suggest, that to a first approximation, 15 wt.% of silica would be necessary to form a 0.5 nm coating on the ∼130 $m^2\ g^{-1}$ of high area rutile, in good agreement with the experimental results.

The alumina-modified samples, prepared by a heteroflocculation method that is known to give a more porous coating [8], showed a much smaller decrease in activity. Even at high alumina loadings (40 wt.%) the rate of propan-2-ol oxidation was reduced by 45% relative to the uncoated material and photogreying was reduced by only 12%. This suggests that, for the preparation conditions used by us, alumina is much less effective at covering the metal oxide surface than silica.

3.2. Measurements of yellowing

Samples of alumina-coated titania and silica-coated titania used in the oxidation and reduction studies were mixed with the organic UV absorbers, BMDBM and benzophenone-3, in C_{12}–C_{15} alkyl benzoate. The correlation between the measured discolouration of the mixtures and the level of inorganic oxide coating on the surface of the particles is shown in Fig. 7a and b. Coating with silica (samples F, H, J and L) decreased the yellowing, measured by *b**, caused by interaction with either BMDBM or benzophenone-3 in a way that paralleled the oxidation and reduction results (Figs. 5 and 6). The decrease in yellowing between ∼1 and 15–20 wt.% silica was followed by a plateau from ∼20 to 40 wt.% loading. However, when the surface was modified by alumina (samples M–P), a large initial *increase* in yellowing was observed at low levels of coating, followed by a small reduction in *b** between 10 and 40 wt.% coating. This is considered further in Section 4.

The addition of a stearate outer-coating to the silica and alumina modified titanias (Fig. 8) caused a further reduction in yellowing. The application of 15 wt.% stearate to a 10.5 wt.% silica-coated titanium dioxide surface produced an additional 40% decrease in *b** (Fig. 8). The titanium dioxide coated with 10.5 wt.% alumina required approximately 25–30 wt.% of stearate to produce the same *b** value as 15 wt.% of stearate on the 10.5 wt.% silica sample. However, in terms of fractional decrease, alumina yellowing decreases by 0.34 units per wt.% of stearate, whereas silica yellowing decreases by only 0.13 units per wt.% of stearate. Extrapolating current trends indicates that a stearate level of ∼33 wt.% would make the silica and alumina catalysts equivalent.

3.3. Infrared spectroscopy of BMDBM adsorbed on titanium dioxide

Infrared spectroscopy was used to probe the nature of the titanium dioxide/organic UV absorber interactions. For convenience and because of the similar functional grouping of

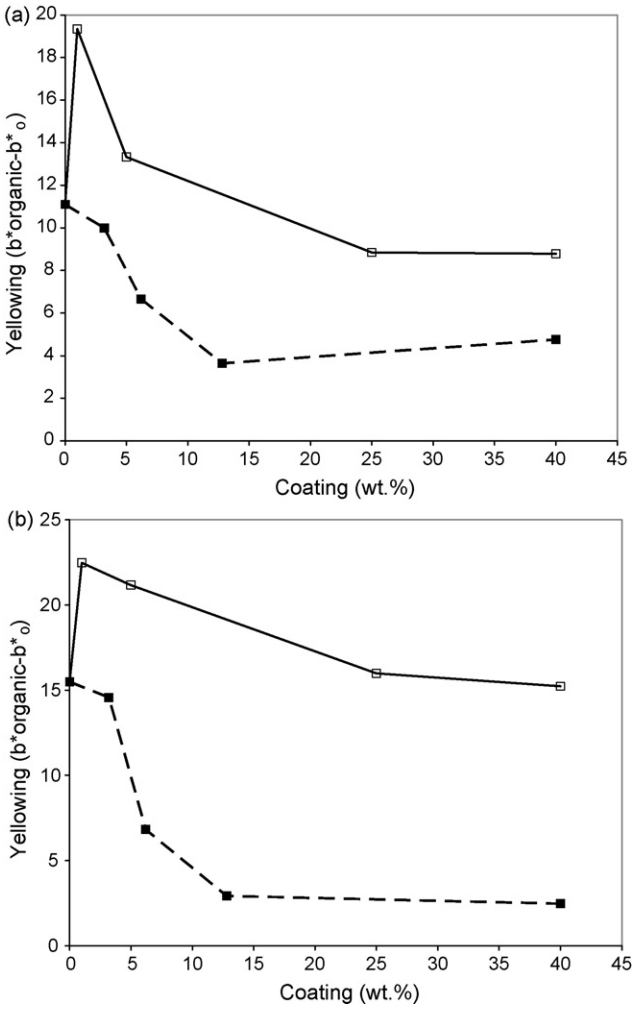

Fig. 7. Yellowing of silica (samples F, H, J and L) (■) and alumina (samples M–P) (□) coated TiO_2, with (a) BMDBM and (b) benzophenone-3.

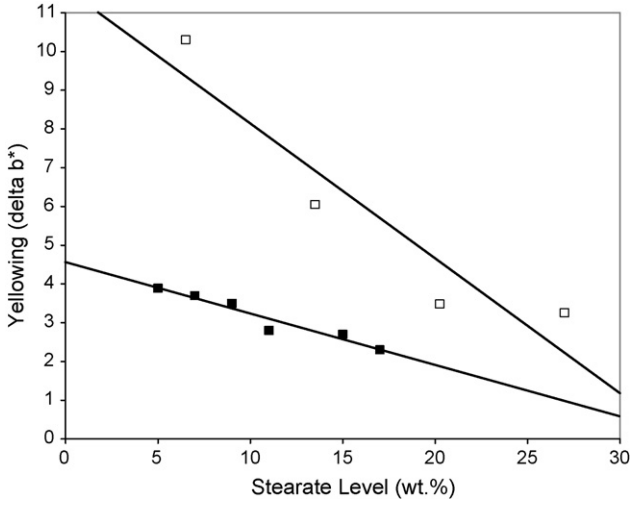

Fig. 8. Dependence of the yellowing of stearate-modified silica (samples Q–V) (■) and alumina (samples W–Z) (□) on the stearate level. In both cases the level of inorganic coating was fixed at 10.5 wt.%.

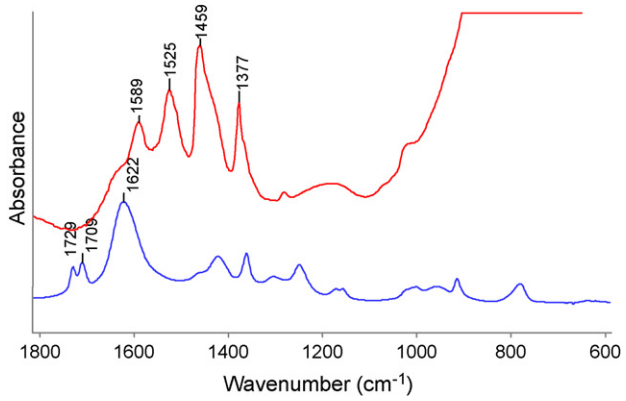

Fig. 9. Spectra of liquid acacH, and acacH adsorbed onto rutile (top line), with the features due to mineral oil removed by subtraction from the latter spectrum.

BMDBM and benzophenone-3, the IR study focused on the adsorption of BMDBM onto titanium dioxide. To aid the assignments of the IR spectra the adsorption of acetyl acetone (acacH) onto uncoated rutile was studied (Fig. 9). The spectrum of liquid acacH displayed absorption derived from both the keto (C=O bands >1700 cm^{-1}) and enol (strong 1622 cm^{-1} band) forms. Adsorption onto rutile downshifted the enol band from 1622 to 1590 cm^{-1} and no keto bands were detected. By contrast, in the IR spectrum of dissolved BMDBM (Fig. 10) there were no detectable keto bands; in fact, the spectrum was dominated by the enol form. Adsorption of BMDBM on the surface of rutile (Fig. 10) yielded bands near 1590, 1530 and 1415 cm^{-1} and the generation of an intense band at 1415 cm^{-1} was observed.

4. Discussion

4.1. The effect of coating on the measured yellowing

The yellowing caused by the interaction of both BMDBM and benzophenone-3 on alumina/TiO_2 and silica/TiO_2 samples followed similar trends. As in earlier studies of propan-2-ol oxidation [1] silica was more effective than an equal weight of alumina coating. It is likely that the poorer coverage of the TiO_2 surface by alumina leads to more yellowing of the dispersions because it allows greater access of the organic UV absorbers to the underlying titanium dioxide. However, at low levels of alumina the coating was seen to induce more yellowing than was measured for the uncoated metal oxide surface (Figs. 7a and b). Morterra et al. [16], in a study of alumina-coated titanium dioxide particles, identified Al^{3+} cations in an alumina surface similar to that examined in this study and it is possible that the presence of small patches of coordinatively unsaturated aluminium on the surface increases the number of sites to which an organic UV absorber can complex. At higher levels of coating, NMR studies on 25 wt.% alumina-coated rutile, sample O, showed that the aluminium were predominantly octahedrally bound with only a small amount (~2%) existing in a tetrahedral coordination. It is probable that at higher levels of alumina fewer coordinatively unsaturated surface sites are available to complex with organic UV absorbers and therefore yellowing of the mixtures is reduced. No initial increase in yellowing was observed for the silica-coated TiO_2. The method of depositing silica leads to a more uniform coherent coating on the surface of the particles with extended cross-linking of Si–O–Si groups at loadings >3 wt.%. This reduces the number of available coordination centres for organic UV absorbers [17].

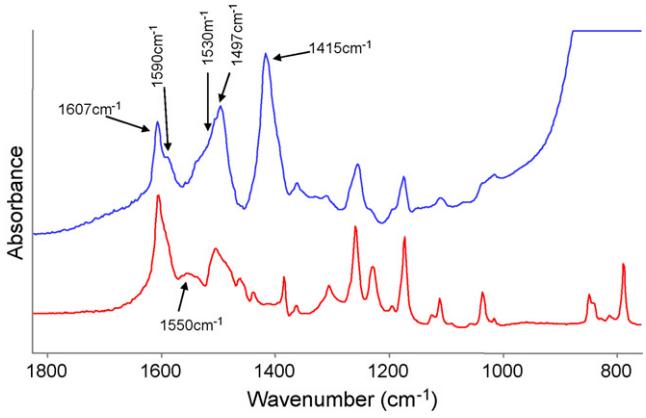

Fig. 10. IR spectra of BMDBM (dissolved in mineral oil), and BMDBM adsorbed onto TiO_2 (top line). In each case, the spectrum of a neat sample of mineral oil was subtracted from the spectrum of interest in order to remove residual solvent bands.

The introduction of an organic (stearate) component to the inorganic coatings leads to a further reduction in yellowing. We have shown previously with similar surface-treated samples that stearate complexes with both Ti and Al surface sites [3]. Furthermore, an unpublished extension of that work identified corresponding silicon/stearate complexes on surfaces coated with silica and stearate. This suggests that the organic component of the coating bonds to Ti, Al and Si, blocking potential yellowing sites available for organic UV absorbers. The larger reduction in yellowing per unit of stearate observed for the alumina stearate-coated titanium dioxide samples is a consequence of the strong coordination of stearate to exposed Ti and Al surface sites.

The importance of covering the metal oxide core particle to minimize yellowing of TiO_2 and organic UV absorber combinations is demonstrated clearly by the linear correlation between both propan-2-ol oxidation versus yellowing and photogreying versus yellowing with BMDBM (Fig. 11a and b). A similar correlation (not shown for brevity) was observed between propan-2-ol oxidation and photogreying and yellowing with benzophenone-3.

4.2. IR spectroscopic identification of the titanium dioxide surface complexes

Initial studies were carried out on the adsorption of acetyl acetone (acacH), which has a similar functional grouping to BMDBM, onto uncoated rutile (sample A). Adsorption of acacH onto rutile yields no keto bands, but the enol band downshifts from 1622 to 1590 cm^{-1}, and strong bands are generated at 1525, 1459 and 1377 cm^{-1} (Fig. 8). It is clear from the literature [18–20] that complexation of acacH to transition metal ions usually leads to strong bands near ~1590, 1530 and 1420 cm^{-1}, though the exact positions can vary considerably. Nakamoto et

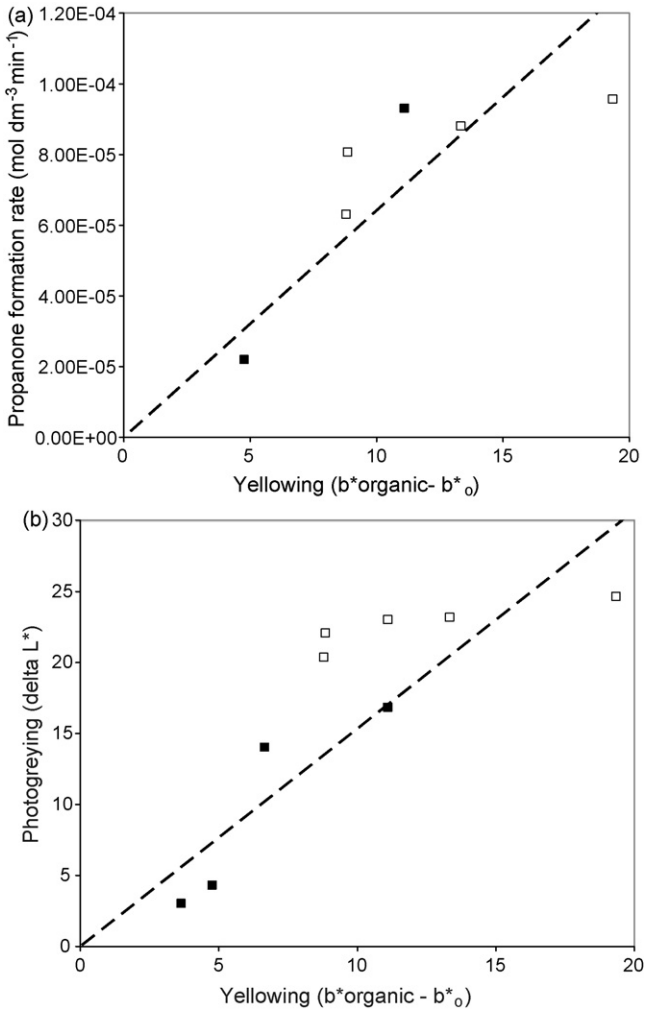

Fig. 11. (a) Propanone formation rate vs. yellowing for silica (samples A and L) (■) and alumina (samples A and M–P) (□) coated TiO_2, with BMDBM. (b) Photogreying vs. yellowing for silica (samples A, H, J and L) (■) and alumina (samples A and M–P) (□) coated TiO_2, with BMDBM.

al. state definitively that the 1590 cm^{-1} band is primarily due to C=C stretching, while the 1520 cm^{-1} band is primarily C=O stretching mixed with C–H bending [18]. Bellamy and Beecher simply state that a band near 1560 cm^{-1} is due to an antisymmetric stretch of the chelate C=O bands, while the 1530 cm^{-1} band is due to the C=C stretch [19]. Yamamoto and Kambara [20] considered that the higher frequency band is probably the C=O stretch, and assigned the 1520 cm^{-1} region to C=C stretch. (Note, in all of these assignments, a C=O or C=C bond really refers to a bond order of ~1.5 rather than 2.) Probably the most conclusive studies have been by Diaz-Acosta et al. [21,22] who used density functional theory (DFT) to calculate the vibrations of $M(acac)_3$ complexes, where M = Sc, Fe, Cr, Al, Ti, V and Mn. This work allowed the vibrations to be assigned with more confidence. In general, bands were predicted between 1590 and 1600, 1520 and 1535 and 1390 and 1430 cm^{-1} for the Cr, Fe and Al complexes, and good agreement was obtained with experiment. Although, experimental data was unavailable for $Ti(acac)_3$ (because the trivalent titanium oxidised too readily to allow good IR spectra to be obtained) the calculated frequencies (and assignments) of $Ti(acac)_3$ were at 1560 cm^{-1} (C=O coupled stretch), 1525 cm^{-1} (C=C + =C–H bend), 1450 cm^{-1} (CH_3 def) and 1406 cm^{-1} (C=O coupled stretch). The authors also predicted a band at 1377 cm^{-1} due to coupled C=O and C=C stretching. They did not comment on the symmetry of the 1560 and 1406 cm^{-1} bands.

It has been shown experimentally that substitution of phenyl rings onto the terminal methyl groups of acac does not drastically shift the vibrations of the complexed anion [23]. Although we cannot directly extrapolate the frequencies calculated for a $Ti(acac)_3$ complex to the case of BMDBM adsorbed to the surface of rutile, they can give useful guidance for the assignment. Therefore, the extent to which a particular oxidation state for the metal, or geometry of the complex, affects the calculated results was investigated by DFT calculations of the vibrations expected for the free acac anion. We used the 6–31 G(d,p) basis set and the B3LYP density functional, with a scaling factor of 0.96 to correct the frequencies. The main IR bands are given in Table 2.

The first three bands in the spectrum of adsorbed acacH onto rutile (Fig. 9) agree very well with our DFT predictions; the 1590 and 1525 cm^{-1} bands are assigned to benzophenone-3 symmetric and antisymmetric stretches of the C=O groups, and the 1460 cm^{-1} band is assigned to the antisymmetric C–C=C stretch. Our calculation did not predict a strong band at 1377 cm^{-1}, but on the basis of common experience a strong methyl deformation is expected in this region. The fundamental disagreement with the work of Diaz-Acosta is in the assignment of the 1530 cm^{-1} band to the antisymmetric C=O stretch (rather than C=C stretch), and the 1446 cm^{-1} band is assigned to the antisymmetric stretch of the C–C=C unit. We also predict that the highest C=O band is due to the symmetric, not antisymmetric stretch, in contrast with previous authors. This calculation illustrates the difficulty in obtaining consistent band assignments between authors. Of course, it is possible that the discrepancy with Diaz-Acosta's work is due to their inclusion of the effect of bonding to a metal. However, despite the disagreements in band assignments, it is strongly indicated that the presence of anionic acac, either free or bonded to a metal, should yield bands at ~1600, 1530 and ~1450 cm^{-1}, although the exact frequency of the latter band can vary widely.

We now turn our attention to the spectrum of BMDBM adsorbed to the surface of rutile, sample A (Fig. 10). The absence of C=O bands near 1730 and 1710 cm^{-1} of the diketone tautomer (Fig. 12a) demonstrates that the enol form of the molecule (Fig. 12b) dominates in solution [24]. Similarly, the absence of a band above 1700 cm^{-1} in the spectrum of adsorbed BMDBM (top line in Fig. 10) rules out the presence

Table 2
Proposed band assignments for ACAC anion predicted from DFT calculations

Scaled frequency (cm^{-1})	Assignment
1612	C=O (symmetric stretch)
1532	C=O (antisymmetric stretch)
1446	C–C=C (antisymmetric stretch)
1415	CH_3 deformation and CH_2 twist

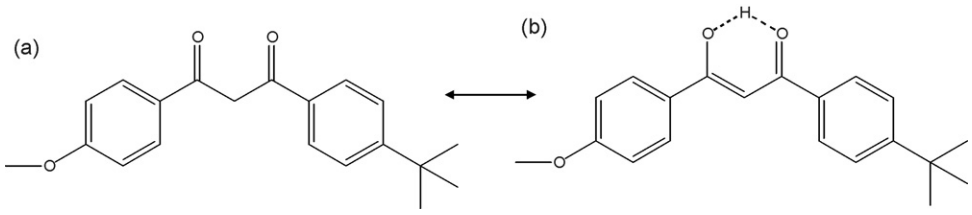

Fig. 12. Diketo (a)–enol (b) tautomerism of butyl methoxy dibenzoylmethane (BMDBM).

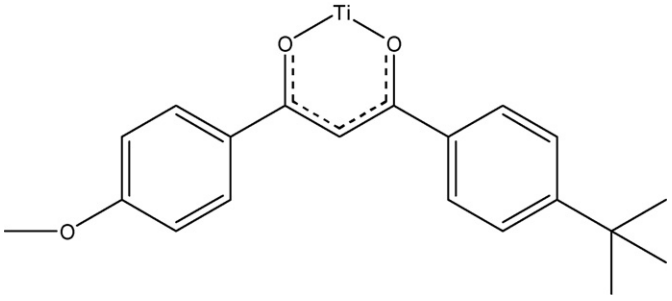

Fig. 13. Proposed BMDBM–Ti complex.

of the keto form of BMDBM and also excludes monodentate coordination of the ligand via just one oxygen, which would yield a distinct C=O band above 1700 cm^{-1}. The presence of a new intense band near 1415 cm^{-1} makes a simple physical adsorption of the enol onto the titania unlikely and points towards chemisorption of the ligand according to Fig. 13. Even though the Ti–O bonds, which would give definitive proof of the formation of a complex, are obscured by the strong TiO_2 absorption below 900 cm^{-1}, the IR spectrum gives strong supporting evidence for the presence of ionised BMDBM on the rutile surface, plus some physisorbed material. By extrapolation of our results for adsorbed acacH onto TiO_2 we have tentatively assigned our principal observed bands as: 1590 cm^{-1} antisymmetric stretch of chelated C=O; 1530 cm^{-1} symmetric stretch of chelated C=O and 1415 cm^{-1} C=C–C antisymmetric stretch. The bands near 1610 and 1497 cm^{-1} are probably due to weakly adsorbed BMDBM in the enol form, but not chelated to the titanium.

5. Conclusion

Surface treatment of nano-particulate titania with silica, or high levels of alumina, reduces the yellowing of mixtures of titania with organic UV absorbers such as benzophenone or BMDBM. More uniform, silica coatings caused a greater reduction of yellowing than the patchier alumina coatings. These results show that the yellowing is caused by an interaction between the titania surface and the organics.

Although obscuration by TiO_2 of the region in which the Ti–O bonds would absorb infrared radiation or scatter Raman light precludes a definitive statement, the IR spectra of adsorbed BMDBM strongly suggest that this interaction is chemisorption of BMDBM as a bidentate anion on the surface titaniums.

Acknowledgements

This work was carried out as part of an EPSRC Industrial CASE collaboration between ICI, Uniqema and Newcastle University. The authors thank Croda (formerly Uniqema) for permission to publish and acknowledge the efforts of Tammy Roza, Daniel Tee and Emma Golden (Industrial placement students at Uniqema) for the preparation and characterisation of materials used in this study.

References

[1] T.A. Egerton, I.R. Tooley, J. Mater. Chem. 12 (2002) 1111–1117.
[2] T.A. Egerton, I.R. Tooley, L.M. Kessell, L. Wang, J. Nanopart. Res. 9 (2) (2007) 251.
[3] T.A. Egerton, N.J. Everall, I.R. Tooley, Langmuir 21 (2005) 3172–3178.
[4] R.P. Elliott, R.K. Gabbi, N.J. Jones, J.C. Cantor, Eur. Patent (Pat. No. EP1602352) (2005).
[5] V.P.S. Judin, Chem. Brit. (1993) 503.
[6] D. Schlossman, Y. Shao, in: N. Shaath (Ed.), Cosmetic Science and Technology Series—Sunscreens, Regulations and Commercial Development, vol. 28, 3rd ed., 2005, pp. 239–279 (Chapter 14).
[7] J.P. Hewitt, Formulating to achieve high UVA protection in sun products, in: Proceedings of The Royal Society UVA Protection Conference, 2001.
[8] T.A. Egerton, KONA Powder Part. 16 (1998) 46.
[9] I.R. Tooley, Ph.D. Thesis, University of Newcastle upon Tyne, 2001.
[10] T.A. Egerton, J.A. Mattinson, J. Photochem. Photobiol. A: Chem. 186 (2007) 115.
[11] G.P. Dransfield, S. Cutter, P.L. Lyth, US Patent (Pat. No. 7101427) (2007).
[12] B.E. Warren, X-Ray Diffraction, Addison-Wesley, 1969, pp. 254–257.
[13] C.F. Bohren, D.R. Huffman, Absorption and Scattering of Light by Small Particles, John Wiley & Sons, New York, 1983.
[14] R.K. Iler, U.S. Patent (Pat. No. 2885366) (1959).
[15] K. McLaren, The development of the CIE 1976 ($L^*a^*b^*$) uniform colour-space and colour-difference formula, J. Soc. Dyers Colour. 92 (1976) 338–341.
[16] C. Morterra, G. Cerrato, M. Visca, M. Lenti, J. Mater. Chem. 2 (3) (1992) 341.
[17] H.C. Bergna, The Colloid Chemistry of Silica, 1st ed., American Chemical Society, 1994, p. 562.
[18] K. Nakamoto, P.J. McCarthy, A.E. Martell, J. Am. Chem. Soc. 83 (1961) 1272.
[19] L.J. Bellamy, L. Beecher, J. Chem. Soc. (1954) 4487.
[20] A. Yamamoto, S. Kambara, J. Am. Chem. Soc. 79 (1958) 4344.
[21] I. Diaz-Acosta, J. Baker, J.F. Hinton, P. Pulay, Spectrochim. Acta A 59 (2003) 363.
[22] I. Diaz-Acosta, J. Baker, W. Cordes, P. Pulay, J. Phys. Chem. A 105 (2001) 238.
[23] K. Nakamoto, Y. Morimoto, A.E. Martell, J. Phys. Chem. 66 (1961) 346.
[24] C.A. Bonda, in: N. Shaath (Ed.), Cosmetic Science and Technology Series—The Photostability of Organic Sunscreen Actives: A Review, vol. 28, 3rd ed., 2005, pp. 329–334 (Chapter 17).